

# INFLUENCE OF MATERIAL PARAMETERS ON THE PERFORMANCE OF NIOBIUM BASED SUPERCONDUCTING RF CAVITIES

Arup Ratan Jana<sup>1,2</sup>, Abhay Kumar<sup>3</sup>, Vinit Kumar<sup>1,2</sup> and Sindhunil Barman Roy<sup>1,2</sup>

<sup>1</sup>Homi Bhabha National Institute, Mumbai 400094, India

<sup>2</sup>Materials and Advanced Accelerator Sciences Division, Raja Ramanna Centre for Advanced Technology, Indore - 452013, India

<sup>3</sup>Design and Manufacturing Technology Division, Raja Ramanna Centre for Advanced Technology, Indore - 452013, India

## *Abstract*

A detailed thermal analysis of a Niobium (Nb) based superconducting radio frequency (SRF) cavity in a liquid helium bath is presented, taking into account the temperature and magnetic field dependence of the surface resistance and thermal conductivity in the superconducting state of the starting Nb material with different impurity levels. The drop in SRF cavity quality factor ( $Q_0$ ) in the high acceleration gradient regime (before ultimate breakdown of the SRF cavity) is studied in details. It is argued that the high field Q-drop in SRF cavity is considerably influenced by the material parameters such as electrical conductivity, and thermal diffusivity. The detail analysis also shows that the current specification on the purity of niobium material for SRF cavity fabrication is somewhat over specified, and an optimally pure Nb material may be good enough. This information will have important implication towards the cost reduction of superconducting technology based particle accelerators for various applications.

## I. INTRODUCTION

One of the remarkable developments in the area of particle accelerators in modern times has been the successful use of the state of the art superconducting radio frequency (SRF) cavities in building high energy linear accelerators (linacs) [1-5]. The phenomenon of superconductivity leads to dissipation less flow of electric current at DC level. However, when ac surface currents flow at the surface of an SRF cavity to create the required electromagnetic field for accelerating the charged particles, there is a relatively small but finite dissipation of heat, which increases with the frequency ( $f$ ) of ac surface current as  $f^2$  [1, 5]. Even then for generating a given value of acceleration gradient  $E_{\text{acc}}$ , the power loss  $P_c$  at the cavity surface in an SRF cavity is significantly small as compared to that in the case of a normal conducting radiofrequency (RF) cavity, when the operating frequency is in the range below  $\sim 3$  GHz. Therefore, the SRF cavities are quite attractive choice for high energy - high current accelerators, operating in the continuous wave (CW) or long pulse mode [5, 6]. The low loss feature of an SRF cavity is characterized by its extraordinary high value of quality factor  $Q_0$  ( $\sim 10^{10}$ ), which is inversely proportional to the power loss  $P_c$  at the cavity wall [1, 5, 7]. The superconducting material used for making the SRF cavity is characterized by its surface resistance  $R_s$  in the superconducting state at the operating frequency. The power loss of an SRF cavity is proportional to  $R_s$ , which implies that  $Q_0$  will be inversely proportional to  $R_s$  [5, 7].

Niobium (Nb) is the material of choice for making SRF cavities because of its relatively high value of superconducting transition temperature or critical temperature  $T_c$  ( $\sim 9.2$  K) as well as the lower critical magnetic field  $B_{c1}$ , relative abundance and ease in availability, and mechanical strength as well as formability. Experimentally, the  $Q_0$  of a Nb-SRF cavity shows the following typical trend with the

increasing strength of the amplitude  $B_a$  of the RF magnetic field at the cavity surface: it first increases slightly in the very low field ( $B_a \sim 0$  to 20 mT), then it decreases gradually in the medium field regime ( $B_a \sim 20$  to 80 mT), and finally, a sharp fall occurs at higher RF fields ( $B_a \sim 80$  to 180 mT), which is known as the  $Q_0$  drop [8, 9]. This sharp fall in  $Q_0$  indicates the breakdown of the superconductivity in the SRF cavity material. The corresponding value of  $B_a$  at which this happens is known as the threshold magnetic field  $B_{th}$ . Theoretically, the limit of the performance of an Nb-SRF cavity is reached when the oscillatory magnetic field (rather magnetic flux-lines) associated with the applied RF field starts penetrating the bulk of Nb material giving rise to the heat dissipation. This is expected to happen at the lower critical field ( $B_{c1}$ ) [10, 11]. In some quarters, it is believed that this dissipation less superconducting response may continue beyond  $B_{c1}$  up to the superheating field  $B_{sh}$  [5]. However, it has been experimentally observed that in Nb-SRF cavities,  $B_{th}$  is often significantly less than the lower critical field  $B_{c1}$  [5].

In earlier days, the high gradient operation of an SRF cavity was mostly limited by the field emission or other synchronous / non-synchronous processes of the electron emission [5, 6]. However, these barriers were surpassed later largely due to the appropriate shaping of the cavity geometry and the advent of chemical surface treatment of the formed SRF-cavity [13]. In recent times, there is a continual quest in the SRF community to push this threshold limit  $B_{th}$  towards  $B_{c1}$  (or beyond) of Nb to achieve a higher value of accelerating gradient  $E_{acc}$ , and simultaneously a higher value of  $Q_0$  to make the higher energy accelerators economically more viable.

More importantly, the observed threshold value  $B_{th}$  of Nb-SRF cavities depends on the quality of the starting Nb material, as well as the processing techniques used during the cavity development. The high purity of the Nb material ensures a higher value of the thermal conductivity  $\kappa$  in the normal state and the cavity processing removes the surface damage of the Nb material, which takes place in the course of forming a SRF cavity. However, at the typical operating temperature of 2K in the superconducting state of Nb, the value of  $\kappa$  reduces significantly. Therefore, the heat removal turns out to be a crucial issue even though the rate of heat generation may be small in the case of an SRF cavity.

In order to realize the goal of high accelerating gradient accompanied with high  $Q_0$ , the prevalent practice followed in the SRF community is to use highly pure niobium, mainly to achieve a higher thermal conductivity [1]. The purity of a metal is often characterized by the residual resistivity ratio ( $RRR$ ), which is usually defined as the ratio of the resistances of the metal at room temperature and at a low enough temperature, where the resistance of the metal has reached its residual resistance limit [1, 5, 6]. Contemporary SRF community has set the value of  $RRR \sim 300$  as the most recommended choice for the niobium material for SRF cavity fabrication. Experimental observations are there both in favor as well as against this empirical choice of standard for  $RRR$  [6]. While for a metal, the increasing purity level results in an improvement in the thermal conductivity, in a superconductor in the clean limit the value of superconducting surface resistance  $R_s$  *increases* with purity as predicted by the BCS theory. Nb metal with  $RRR$  value greater than 50 is expected to be in the clean limit of superconductivity, and the increase in  $R_s$  with the increase in  $RRR$  value beyond 50 has actually been observed experimentally [12]. Therefore, for a high purity material, although the rate of heat conduction will increase, this advantage may be countered by the fact that there will be *more* heat generation at the cavity surface. A rigorous calculation of the heat transfer problem will therefore be needed to find out the amplitude  $B_a$  of magnetic field at the surface of the cavity at which the thermal breakdown of superconductivity occurs in the cavity for a given grade of purity of the starting Nb material for SRF cavity fabrication. More importantly,  $R_s$  is also influenced by the magnetic field  $B_a$ .

Hence, it is no longer only a thermal phenomenon, but a *magneto-thermal* phenomenon [10, 13]. A theoretical analysis to calculate the breakdown field has been performed in Refs. [14, 15], where  $R_s$  is assumed to be independent of  $B_a$ , and is a function of temperature alone. Weingarten [16] and Gurevich [17] have taken exponential dependence of  $R_s$  on  $B_a$  into account, and have performed more rigorous analyses of the thermal breakdown phenomenon. The experimentally observed breakdowns have also been explained by some authors on the basis of local effects like the hot spot generation at the sites of inclusions of other materials in the SRF cavity surface, defects generated at the welding region of the SRF cavities and micro cracks on the SRF cavity surface. These are, however, extraneous sources of heat dissipation usually introduced during the fabrication of the SRF-cavity, and can be avoided by improvement in the method of SRF cavity fabrication and post processing of SRF cavity.

Most of these analyses of the thermal breakdown phenomena did not consider the temperature dependence of the thermal conductivity  $\kappa$  of niobium in spite of the same being significant. Although the analysis presented in the Ref. 17 considered this dependency, it did not take the dependency of the surface resistance  $R_s$  on  $B_a$ . A more rigorous approach will therefore be to include the dependence of temperature on  $\kappa$ , and dependencies of magnetic field as well as temperature on  $R_s$  in the analysis, for different purity levels of niobium. In this paper, we have followed this approach to perform a theoretical analysis of this *magneto-thermal* process. Since the  $R_s$  and  $\kappa$  depend on  $T$  and  $B_a$ , and the temperature profile itself depends on the heat source decided by the  $R_s$ , as well as heat diffusion decided by  $\kappa$ , the problem needs to be solved in a self-consistent manner. We have performed such a self-consistent analysis, and calculated the steady state temperature profile inside the material of the Nb SRF-cavity. Knowing the temperature of the inner surface of the SRF cavity, the surface resistance and therefore the  $Q_0$  value is evaluated as a function of  $B_a$  for different purity levels of the cavity material. As discussed earlier, improving the purity level of Nb improves the  $\kappa$ , which is favorable for the performance of an SRF cavity. This is, however, at the cost of more heat load arising due to the rise in surface resistance with the increasing level of the purity of the Nb material. The optimum value of the purity level and therefore the optimum value of the material parameters are thus decided by a trade-off between these two competing processes. Our analysis models these two processes rigorously by taking the temperature and magnetic field dependence of  $R_s$  and  $\kappa$ . This methodology is then used to optimize the material purity level to enhance the performance of an SRF cavity.

To the best of our knowledge, such an analysis has not been performed in the past. We believe that it is important to perform this kind of analysis rather than specifying a high value of purity of the starting Nb material for SRF cavity fabrication on an ad-hoc basis.

The analysis presented in the paper is for the frequency 650 MHz, which has been chosen as the operating frequency for the elliptic SRF cavities of the injector linac for the proposed Indian Spallation Neutron Source (ISNS) project [18, 19]. In the present work, attempts are made to find a rationale for specifying the optimum purity level of the starting niobium materials used for fabrication of 650 MHz SRF cavities. An important aim here is to investigate whether the high purity niobium having RRR  $\sim 300$  (which is relatively expensive compared to lower RRR grade niobium) is really necessary for SRF cavity development. The paper is organized as follows. SECTION II discusses the analytical models used to calculate the thermal conductivity  $\kappa$  and superconducting surface resistance  $R_s$  as a function of (i) the purity level of the Nb material, (ii) RF magnetic field amplitude  $B_a$  at the cavity surface, and (iii) temperature  $T$ . Next, in SECTION III, we present the results of our magneto-thermal analysis, where we highlight the influence of the purity level of niobium in the

electromagnetic response of an Nb-SRF cavity. Finally, in SECTION IV, we discuss the important inferences that can be drawn from the analysis presented in the paper, and conclude.

## II. THEORETICAL FORMULATION

### II.A. Generalities

The quality factor  $Q_0$  of an SRF cavity is a measure of the amount of RF power  $P_c$  dissipated at the cavity wall corresponding to the electromagnetic energy  $U$  stored inside the cavity [8]. Mathematically, it is expressed as  $Q_0 = \omega U / P_c$ , where  $\omega$  is  $2\pi$  times the RF frequency  $f$ . Here, denominator is the time averaged power loss  $P_c$  that can be expressed as  $R_S \int_S B_a^2 ds / (2\mu_0)$ , where  $\mu_0$  is the permeability of free space, and the integration is carried over the inner surface area of the SRF cavity. Hence, the quality factor can be expressed as:

$$Q_0 = \frac{\omega U}{R_S \frac{\int_S B_a^2 ds}{2\mu_0}} = \frac{G}{R_S}. \quad [1]$$

Here, the factor  $G = 2\mu_0\omega U / \int_S B_a^2 ds$  is known as the geometry factor. Its value depends only on the cavity geometry [5, 8]. Therefore, the functional dependency of the quality factor can be expressed as  $Q_0 \propto 1/R_S$  for a fixed cavity shape. The factor  $G$  is independent of the field applied. If we assume that  $R_S$  is field-independent, then  $Q_0$  will have a very weak dependency on  $B_a$ , and should remain nearly constant up to the breakdown limit. But the experimentally observed quality factor is associated with a  $Q_0$ -slope. Also, the breakdown does not occur at a sharp value of  $B_a$ , instead it occurs over a range of  $B_a$ . This implies that  $R_S$  should have some direct or indirect functional dependency on  $B_a$  [15, 16]. This will be discussed in the next sub section.

It may be in order to present here a brief discussion on the purity level of the material. For niobium, mostly the defects are of two types –(ii) impurities due to metallic (e.g., Ta, Fe, Sn *etc.*) or non-metallic (e.g., O, H *etc.*) inclusions, and (ii) various kinds of material defects including dislocations [20]. Amongst the metallic impurities, tantalum (Ta), being the chemical neighbor of Nb, is present in the starting mineral ore from which Nb is separated out. Since it is a substitutional impurity, it does not have much influence on the electronic properties of the bulk niobium [5]. Following an expensive processing and purification process of the niobium material, the presence of Ta is reduced to the *ppm* level. Besides, because of the proximity effect, small Ta inclusions surrounded by the vast amount of Nb neighbours might not affect the superconducting response of the Nb-SRF cavity surface. The other class of defects, *i.e.*, dislocations, is unavoidable even in very pure Nb with low Ta impurity level. The amount of such defects will actually increase during the half-cell formation of an elliptical Nb-SRF cavity, and thus the *RRR* of the Nb material in a finished product of Nb-SRF cavity will be significantly different from the *RRR* of the starting Nb material. In general, the electronic mean free path ( $l_e$ ) of a metal is a function of the purity level of that material [5,11,16]. The normal state electrical resistivity ( $\rho_{no}$ ) of a metal can be estimated from the value of the mean free path  $l_e$ . For niobium, at  $T_c \sim 9.2$  K, we can write  $l_e = (3.7 \times 10^{-16} \text{ ohm} \cdot \text{m}^2) / \rho_{no}$  [20], following the SI units. We would like to emphasize that for the normal electrons, the value of  $\rho_{no}$  as well as  $l_e$  remain almost unaltered in Nb in the temperature range below  $T_c$ . As already mentioned, the commonly followed approach to quantify the purity level in Nb is in terms of *RRR*, which is the ratio between the resistivity  $\rho_{300K}$  at 300 K and the normal state resistivity ( $\rho_{no}$ ) at a sufficiently low temperature, say at 9.2 K, *i.e.*, just above the superconducting transition temperature. Therefore, the *RRR* will be proportional to  $l_e$ . In the next sub sections, we will explain how the level of impurity plays an important role in deciding the  $R_S$  and  $\kappa$  of a material.

### II.B. Electrical surface resistance ( $R_S$ )

In the zero-field condition, *i.e.*,  $B_a = 0$ ,  $R_S$  of a superconducting material is obtained from the BCS formulation, and is expressed as

$$R_S(\omega, T) = R_{BCS}(\omega, T) + R_i = \mu_0^2 \omega^2 \sigma_{no} \lambda^3 \frac{\Delta_0}{k_B T} \ln\left(\frac{\Delta_0}{\hbar\omega}\right) \exp\left(-\frac{\Delta(T)}{k_B T}\right) + R_i. \quad [2]$$

Here,  $k_B$  and  $\hbar$  are the Boltzmann constant and reduced Planck constant respectively,  $\Delta_0$  and  $\lambda$  are the zero-temperature superconducting energy gap and the field penetration depth at temperature  $T$  respectively. In terms of the London penetration depth ( $\lambda_L$ ),  $\lambda$  can be expressed as  $\lambda \approx \lambda_L \sqrt{1 + \xi_0/l_e}$  [11], where  $\xi_0$  is the coherence length of a pure superconducting material. The parameter  $\sigma_{no}$  is the normal state conductivity of the superconducting material at a temperature  $T$ . As we have discussed in the previous sub section,  $\sigma_{no} \propto l_e$ .

As discussed above, both  $\sigma_{no}$  and  $\lambda$  are dependent on  $l_e$ . Therefore, in order to highlight the effect of material purity on the surface resistance, we separate the  $\sigma_{no}$  and  $\lambda$  dependent part from the expression of  $R_{BCS}$ , which is expressed in terms of  $l_e$  as follows:

$$R_{BCS} \sim \left(1 + \frac{\xi_0}{l_e}\right)^{\frac{3}{2}} l_e. \quad [3]$$

Figure 1 shows the plot of  $R_{BCS}(T, l_e)$  normalized to its minimum value, as a function of  $l_e$ . Here, we have used  $\xi_0 \sim 38 \text{ nm}$  for Nb [16].

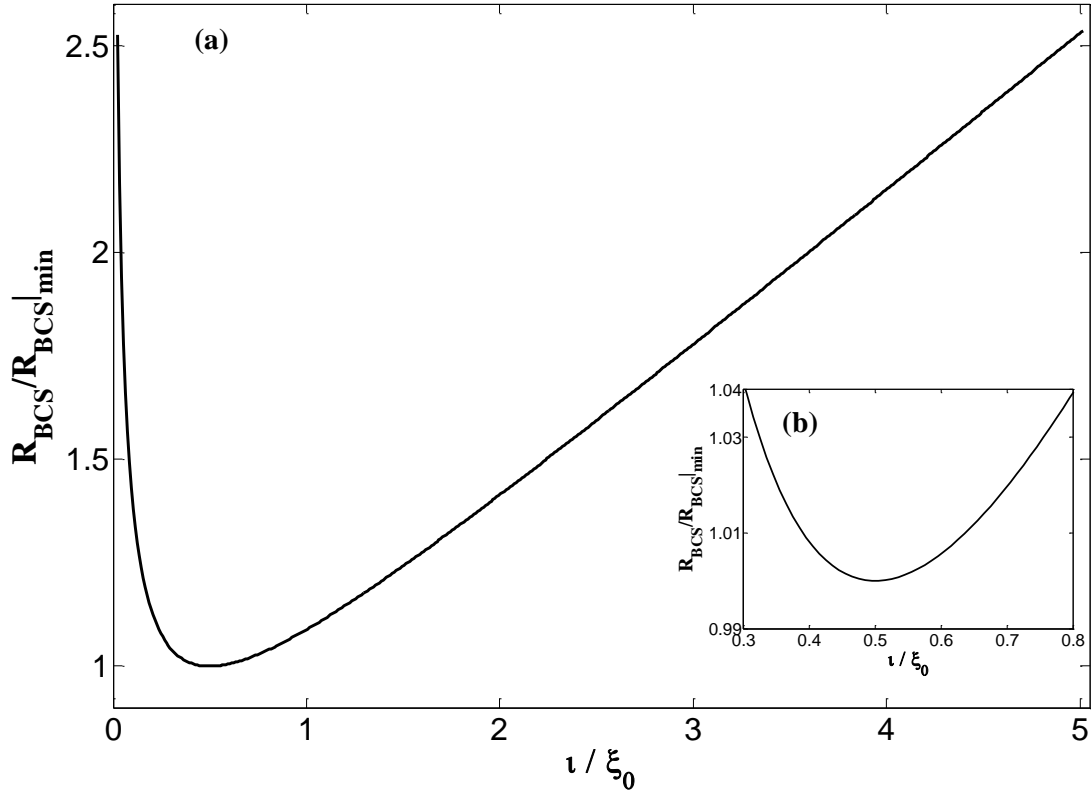


Fig.1: (a) Plot of the normalized  $R_{BCS}$  at 2 K as a function of  $l_e/\xi_0$  for niobium. (b) Inset is the zoomed view of the minima which corresponds to  $l_e/\xi_0 \sim 0.5$ .

We observe that the dependency of  $R_{BCS}$  on the impurity level of the material is not monotonic: in the clean limit of superconductivity, *i.e.*,  $l_e/\xi_0 \gg 1$ ,  $R_{BCS} \propto l_e$ , whereas in the dirty limit, *i.e.*,  $l_e/\xi_0 \gg 1$ ,  $R_{BCS} \propto 1/\sqrt{l_e}$ . Typically, the starting niobium materials used for the fabrication of a SRF cavity has its purity level in the clean limit. Therefore, with the increasing level of purity,  $R_{BCS}$  also increases, resulting in an increased heat load. Here, the term  $R_i$  in the right side of Eq. (2) is known as the residual resistance. Unlike the first term on the right side of Eq. (2), this term is present even at zero temperature and has its origin in trapped magnetic flux, formation of niobium hydride islands near the surface *etc.* [11]. Note that although the term “residual resistance” in Eq. (2) may appear

similar to residual resistance in the definition of  $RRR$ , they are completely different and independent of each other. The term *resistance* in “residual resistance  $R_i$ ” actually denotes the surface resistance [7]. Based on the experimentally observed values, we have assumed a value of  $10 \text{ n}\Omega$  for  $R_i$  in our analysis. A precise estimation for the surface resistance as a function of the temperature and the purity level of the superconducting Nb material can be obtained with the help of Eq. (2). As discussed earlier, these dependencies alone cannot explain why the threshold value of the magnetic field  $B_{\text{th}}$  is well below the critical magnetic field, as predicted by the BCS theory. It is important to consider a modified expression for  $R_S$  in the presence of an applied RF magnetic field  $B_a$  for a more rigorous analysis. Following the work of A. Gurevich [17], for a type-II superconductor in the clean limit, the modified  $R_S(T, l_e, B_a)$  can be written as follows:

$$R_S = \frac{8R_{BCS}(l_e)}{\pi\beta_0^2} \int_0^\pi \sinh^2\left(\frac{\beta_0}{2}\cos\tau\right) \tan^2\tau d\tau + R_i, \quad [4]$$

where,  $\beta_0 = \frac{\pi}{2^{3/2}} \frac{B_a}{B_c} \frac{\Delta}{k_B T}$ . The dependency of  $R_S/R_{BCS}$  as a function of the parameter  $\beta_0$  is shown in Fig. 2. Here,  $B_c$  is the thermodynamic critical magnetic field. In our calculation, we used  $B_c = 200 \text{ mT}$  for Nb [17].

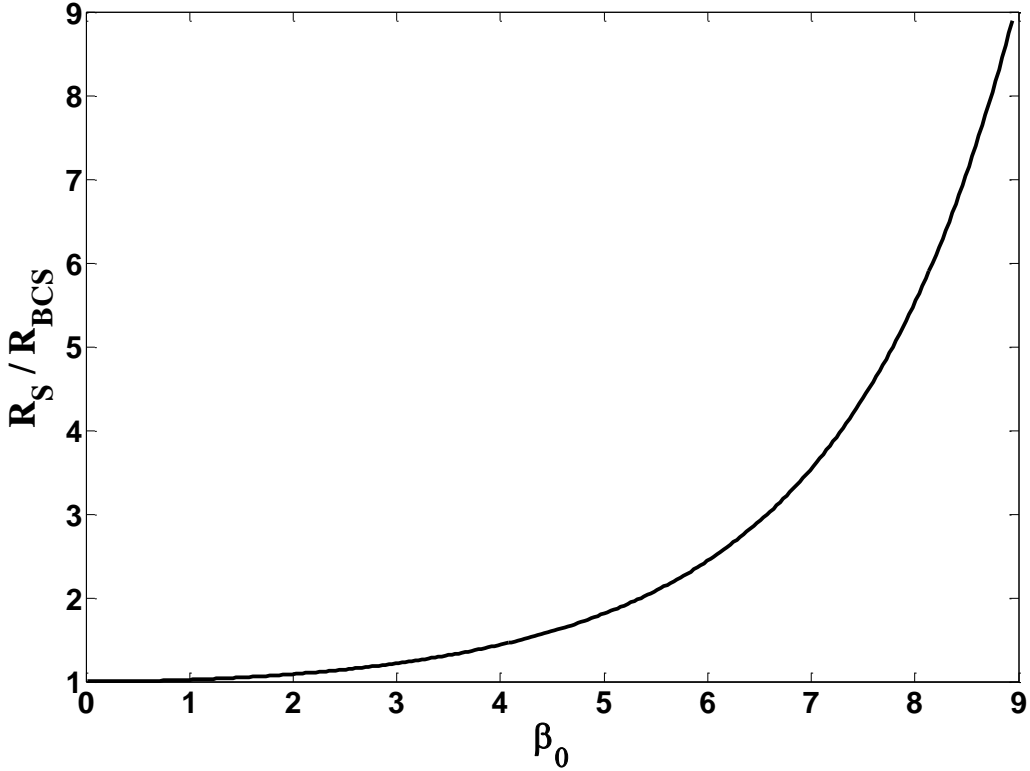


Fig. 2: Plot of normalized  $R_S$  as a function of  $\beta_0$ .

In the high field limit, Eq. (4) can be written in an approximate form as follows:

$$R_S \approx \frac{4R_{BCS}}{\beta_0^3 \sqrt{2\pi\beta_0}} e^{\beta_0} + R_i. \quad [5]$$

This shows that in the high field, superconducting energy gap  $\Delta$  will be reduced as  $\Delta_{\text{eff}} = (1 - \pi B_0 / B_c 2^{3/2}) \Delta$ . This modification in the energy gap will accelerate the effective breakdown phenomena.

In this subsection, we have discussed the dependency of  $R_S$  on temperature, applied magnetic field and the purity level of the material. During the operation of an SRF cavity, the heat generated at the SRF cavity wall is quantified in terms of  $R_S(T, B_a, l_e)$ , and heat will then be conducted through the thickness of the SRF cavity wall depending on the thermal conductivity  $\kappa$  of the material. In the next sub-section, we will discuss the dependence of thermal conductivity of niobium on different parameters, in the superconducting state.

### II.C. Thermal conductivity of the SRF cavity material

There are two types of heat carriers in a metal - the conduction electrons, and the lattice vibrational modes *i.e.*, phonons [21]. Amongst these two, the electronic contribution dominates. The total thermal conductivity of a metal  $\kappa(T)$  is the summation of these two contributions, *i.e.*  $\kappa(T) = \kappa_{en}(T) + \kappa_L(T)$  [22, 23]. The electronic contribution  $\kappa_{en}(T)$  arises because of the scattering of normal electrons from lattice imperfections due to the thermal vibrations as well as various defects (including impurities) present in the material [23], which can be estimated using the Wiedemann-Franz law (at low temperatures), which is stated as  $\kappa_{en} = L_0 \sigma_{no} T$  [21], where,  $L_0$  is the Lorentz number. Considering the contribution from the electron - lattice scattering *i.e.*  $\kappa_{el} = 1/aT^2$ , where  $a$  is constant, the total electronic thermal conductivity can be written as  $\kappa_{en}(T) = (1/L_0 \sigma_{no} T + aT^2)^{-1}$ . As discussed in the previous paragraph, with the increase in the purity level of the material, its electrical conductivity  $\sigma_{no}$  increases and so does the  $\kappa_{en}(T)$ . Hence, the material in its purest form will offer the best thermal conductivity.

In the superconducting state of a metal, the number of free electrons reduces because of the formation of cooper pairs. This results in a scaled down contribution in the electronic thermal conductivity  $\kappa_{es}(T)$  of a superconductor. This scale factor  $R(y)$ , as given by Bardeen-Rickayzen-Tewordt [24] is as follows:

$$\frac{\kappa_{es}}{\kappa_{en}} = R(y) = \frac{1}{f(0)} \left[ f(-y) + y \ln(1 + \exp(-y)) + \frac{y^2}{2(1 + \exp(-y))} \right], \quad [6]$$

where  $f(-y)$  is the Fermi integral, and is defined as  $f(-y) = \int_0^{\infty} (z/[1 + \exp(z + y)]) dz$ , and  $y = \Delta(T)/2k_B T$ . Figure 3 shows a plot of  $R(y)$  as a function of temperature.

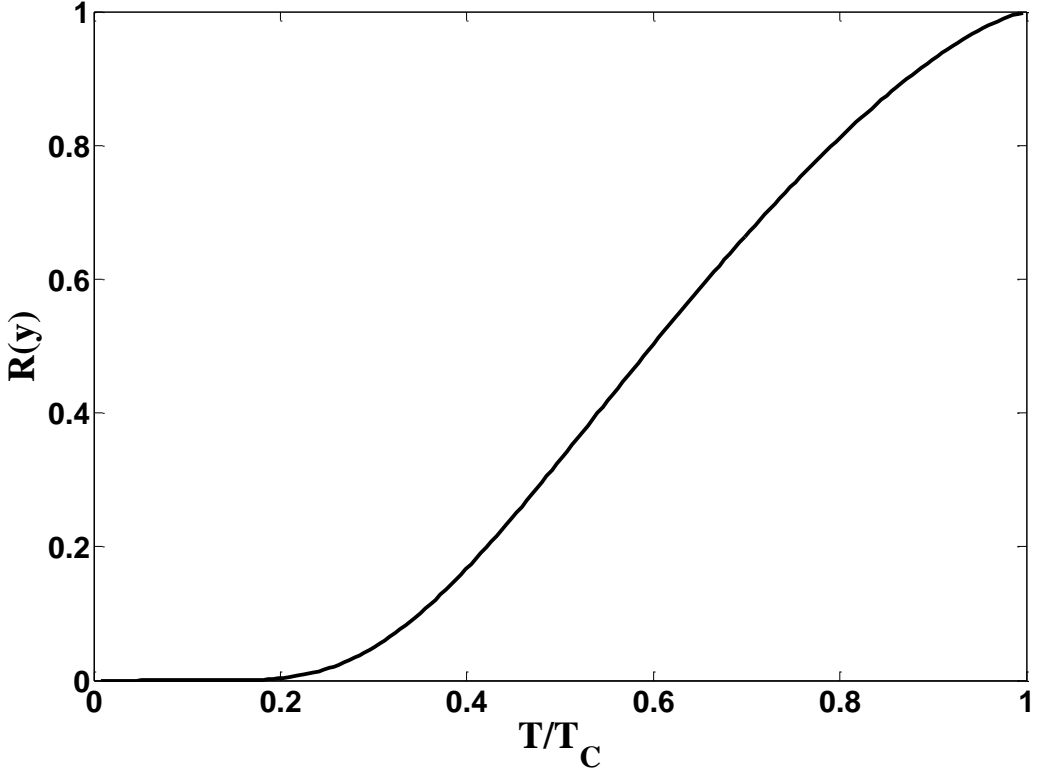


Fig. 3: Plot of  $R(y)$  as a function of  $T/T_C$ .

In our analysis, we have estimated  $\kappa_{en}$  for different values of the impurity levels *i.e.*, for different values of  $\sigma_{no}(l_e)$ , and to calculate the normal state thermal conductivity of Nb at 9.2 K, we have used  $L_0 = 2.45 \times 10^{-8} \text{ W K}^{-2}$  [21,22] and  $a = 7.52 \times 10^{-7} \text{ m W}^{-1} \text{ K}^{-1}$  [23] respectively.

Unlike the free electrons, crystal lattice contributes in a relatively small amount in the total thermal conductivity. The total  $\kappa(T)$  for a material in its superconducting state can be estimated from the following equation [22, 25]:

$$\kappa(T) = \kappa_{es}(T) + \kappa_L(T) = R(y) \left( \frac{1}{L\sigma_{no}T} + aT^2 \right)^{-1} + \left( \frac{1}{DT^2 e^y} + \frac{1}{Bl_{ph}T^3} \right)^{-1}. \quad [7]$$

Here, the second part in the right-hand side is due to the lattice contribution  $\kappa_L(T)$ , where,  $D$  and  $Bl_{ph}$  are the two constants, and  $l_{ph}$  is the phonon mean free path. The values of these two constants depend on different levels and types of post processing [25] that the cavity has undergone. For a defect-free metal with high purity, there is the likelihood of a phonon peak at a very low temperature (around  $T \sim 2$  K), which can result in an enhancement in  $\kappa(T)$ . However, for a non-annealed SRF cavity, defects and dislocation introduced during the process of forming a SRF cavity destroys the phonon peak, partly or sometimes completely. These conditions however improve with the post-processing of an SRF cavity.

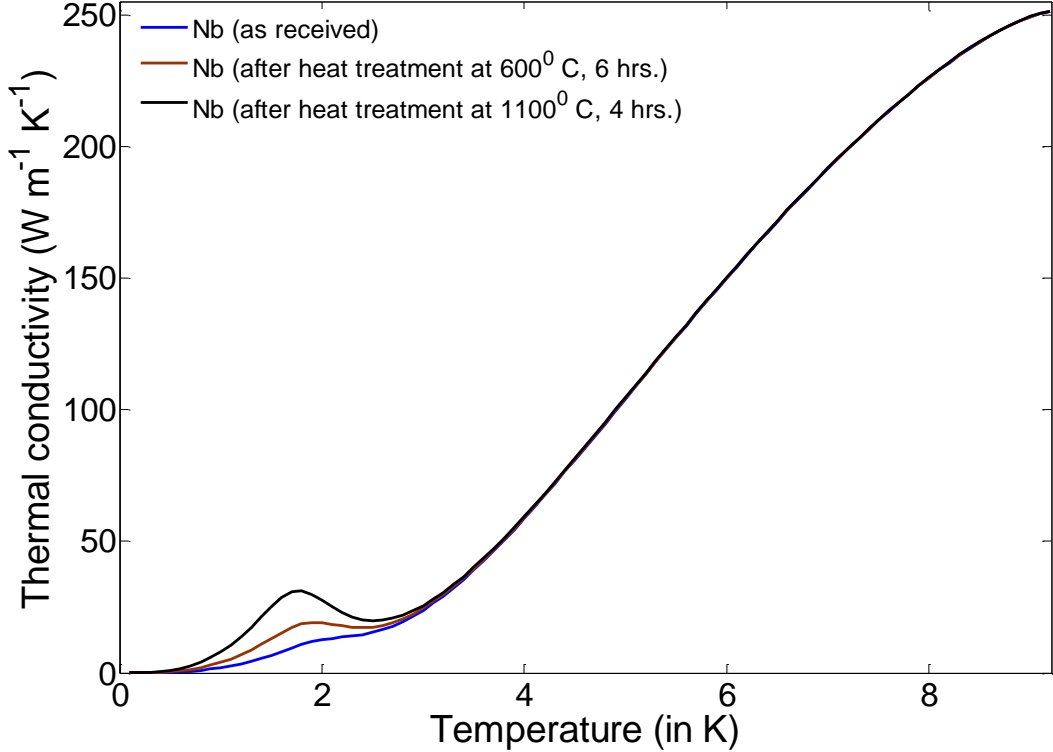


Fig. 4: Total thermal conductivity  $\kappa(T)$  as a function of the temperature ( $T$ ). Contribution from the phonon peaks near 2 K is clearly seen for three different cases [25].

Figure 4 shows the total thermal conductivity of niobium samples, which have undergone three different stage of post-processing – (i) case I, which is the factory received material, (ii) case II, where the sample has undergone a heat treatment at  $600^0\text{C}$  for 6 hrs., and (iii) case III, where the sample has undergone a heat treatment at  $1100^0\text{C}$  for 4 hrs. The parametric data for  $D$  and  $Bl_{ph}$  in Eq. (4) were taken from Ref. [25]. Near 2 K, a small contribution in the total thermal conductivity of the material  $\kappa(T)$  arises because of the partially destroyed phonon peak for the factory received material. Here, we have used  $D = 400 \text{ m K}^3 \text{ W}^{-1}$  and  $1/Bl_{ph} = 0.5 \text{ m K}^4 \text{ W}^{-1}$  for case I. The other two curves show the improvement in the value of  $\kappa(T)$  after the sample has gone through two different post processing sequels [25]. For case II, the values of  $D$  and  $1/Bl_{ph}$  were taken as  $350 \text{ m K}^3 \text{ W}^{-1}$  and  $0.25 \text{ m K}^4 \text{ W}^{-1}$  respectively. Similarly, for case III, we took  $D = 300 \text{ m K}^3 \text{ W}^{-1}$  and  $1/Bl_{ph} = 0.125 \text{ m K}^4 \text{ W}^{-1}$ . Note that based on the practical considerations, case III is not of much relevance [8].

As it is expected, improvement in  $\kappa(T)$  is more effective if we keep the liquid helium bath temperature  $T_B = 2 \text{ K}$ . The phonon peak has almost no effect if we consider  $T_B$  to be equal to 4.2 K.

The thermal conductivity of Nb is dependent on the applied RF magnetic field. However, we did not incorporate this dependency in our calculation. This is because in a superconducting cavity, the RF electric and magnetic fields almost vanish in the bulk of the material. Therefore, in our calculation, we have used the thermal conductivity values considering *zero*-magnetic field condition. In this section, we have discussed the functional dependency of  $R_S$  and  $\kappa$  on  $T$ ,  $B_a$ , and the purity level of the material. As described earlier, heat generated at the inner wall of a SRF cavity diffuses through the wall thickness, and is finally dissipated to the liquid helium bath maintained at  $T_B = 2 \text{ K}$  (or 4.2 K). In this diffusion process, a significant amount of thermal resistance arises because of the relatively small value of  $\kappa$  for the superconducting niobium. Also, the Kapitza resistance that is developed at Nb-He

bath interface contributes prominently in the low temperature regime, causing a temperature jump  $\Delta T = (T_S - T_B)$  across the interface, where,  $T_S$  is the temperature of the cavity outer wall. The value of  $\Delta T$  decides the amount of heat flow  $\bar{Q}$  per unit interface area per unit time, given by  $\bar{Q} = h_k(T_S - T_B)$ . Here,  $h_k$  is the Kapitza conductance, which is a function of  $T_S$  and  $T_B$ . It is estimated in the unit of  $\text{W m}^{-2} \text{K}^{-1}$  from the following equations [26, 27]:

$$h_k = \begin{cases} 200T_S^{4.65} \left[ 1 + 1.5 \left( \frac{T_S - T_B}{T_B} \right) + \left( \frac{T_S - T_B}{T_B} \right)^2 + 0.25 \left( \frac{T_S - T_B}{T_B} \right)^3 \right] & \text{for } T_B \sim 2 \text{ K [26]} \\ 12300(T_S - T_B)^a, \text{ where } a \sim 0.45 \text{ for } T_B \sim 4.2 \text{ K [27].} \end{cases} \quad [8]$$

Amount of heat generated at the inner wall of the cavity is entirely dissipated at the helium bath in the steady state, and a stationary temperature profile is established throughout the material. Therefore, the heat balance equation in the steady state condition is written as:

$$\frac{1}{2\mu_0^2} R_s(T_{so}, B_a, l_e) B_a^2 = -\kappa(T, l_e) \nabla(T) = h_k(T_S - T_B) \quad [9]$$

Here,  $T_{so}$  is the steady state temperature of the cavity inner wall.

### III. NUMERICAL CALCULATIONS AND ANALYSIS OF RESULTS

In this section, we discuss the analytical results of our magneto-thermal analysis, where the purity level of the material is considered as an input parameter. In this analysis, the inner surface of SRF cavity is the source of the outward heat flux, which is then diffused through the thickness of the wall, and is finally dissipated in the liquid helium bath maintained at a constant temperature  $T_B$ . The amount of heat flux depends on  $R_s(T, B_a, l_e)$ , and the rate of heat diffusion is controlled by  $\kappa(T, l_e)$  as well as  $h_k(T, T_B)$ . The calculation of  $R_s$ ,  $\kappa$  and  $h_k$  is performed using the formulation described in the previous section. We then use Eqs. (8) and (9) to find out the temperature of the cavity inner surface in the steady state. The surface resistance  $R_s$  is evaluated at this temperature, including the effect of  $B_a$ , for the given value of  $l_e$ . The quality factor  $Q_0$  is then calculated using this value of  $R_s$  in Eq. (1).

We first describe the calculation for the simple case, where  $\kappa$  and  $h_k$  are treated as constant, *i.e.*, independent of temperature. Such a calculation has been earlier performed by Ciovati [25], where  $R_s$  is treated as a function of temperature alone, and its dependence of magnetic field is not taken into account. We first reproduced the analysis presented by Ciovati [11], which was performed for 1.5 GHz, and then extended it by including the effect of  $B_a$  on  $R_s$ . We observe that the inclusion of the effect of  $B_a$  on  $R_s$  has an important implication, as seen in Fig. 5, where we have plotted  $Q_0$  as a function of  $B_a$  [17] for the two cases – first, without taking the effect of  $B_a$  on  $R_s$ , and second, taking the effect of  $B_a$  on  $R_s$ . Following Ref. [11], in these calculations, we have taken  $\sigma_{no} \sim 3.3 \times 10^8 \Omega \text{ m}^{-1}$ ,  $\kappa \sim 10 \text{ W m}^{-1} \text{ K}^{-1}$  and  $h_k \sim 5 \text{ kW m}^{-2} \text{ K}^{-1}$ . Note that here  $\kappa$  and  $h_k$  values were taken as constant. The nonlinear dependency of  $R_s$  is strongly reflected in the second case. The medium and high field  $Q_0$  slope increases when we include the effect of  $B_a$  on  $R_s$ , and also the breakdown starts at a relatively lower value of the applied magnetic field.

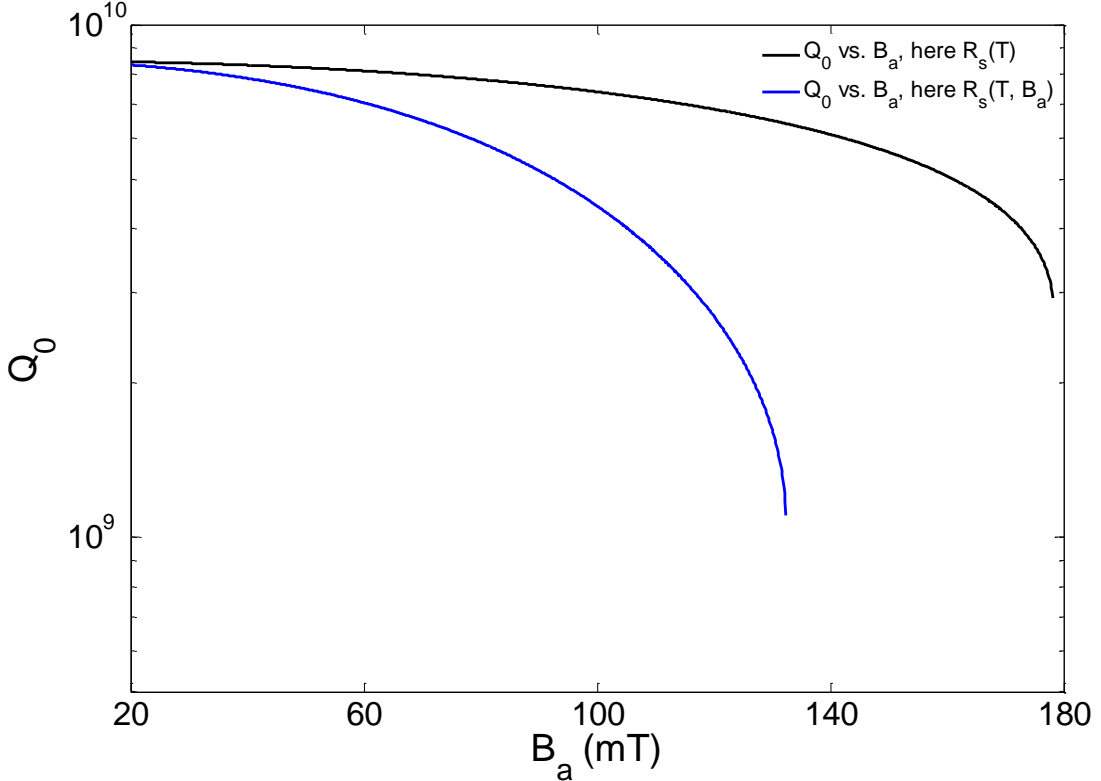


Fig. 5: Plot of  $Q_0$  as a function of  $B_a$ . Here, linear  $R_s$  was calculated following Ref. [11] (in black), and the nonlinear  $R_s$  was calculated following Ref. [17] (in blue).

In the remaining part of this section, we perform the calculations for a 650 MHz elliptical SRF cavity, taking the functional dependency of  $\kappa$  and  $h_k$  into account. We first described the details of problem modeling, followed by presentation of results of numerical calculations in two sub-sections.

### III. A. Simulation model:

Fig. 6 (a) describes the MODEL-I, which is a 4 mm thick infinite Nb slab with planar geometry. One side of this slab is exposed to a spatially uniform RF field resonating at 650 MHz, whereas the other side is in contact with liquid helium at a bath temperature  $T_B$ . From the symmetry of the problem, the heat diffusion equation will be one dimension (1D) here.

MODEL-II describes the three-dimensional (3D) model of a 650 MHz elliptic SRF cavity half-cell [18-19, 29], shown in Fig. 6 (b). Considering the axially symmetric aspect, only a  $15^0$  sector of the half-cell with 4 mm wall thickness was modeled to minimize the computational effort. The field profile used in the calculation is also shown in Fig. 6 (b), which was obtained from the electromagnetic eigen-mode analysis of the cavity. Here also, the temperature of the cavity outer wall is kept fixed at  $T_B$ .

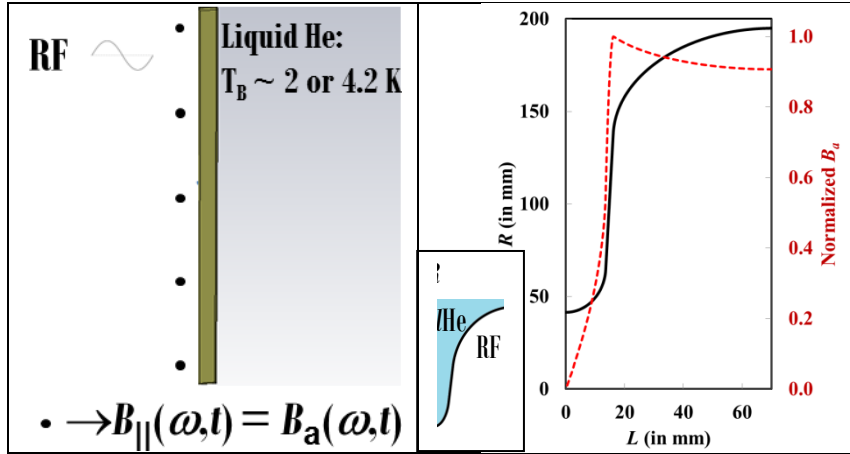


Fig. 6: (a) Geometry of a 4 mm thick infinite plate used as MODEL-I. (b) Elliptic half-cell geometry used in MODEL-II, along with the surface magnetic field (normalized) profile.

### III.B. Numerical calculations and results

In order to estimate the steady state solutions for the converged values  $R_s$  and  $\kappa$ , computer programs were written in MATLAB, and using ANSYS<sup>®</sup> APDL. For the planar geometry, *i.e.* for MODEL-I, where the problem is one-dimensional, MATLAB programs were used. On the other hand, to solve the three-dimensional heat diffusion equation in MODEL-II, we have used ANSYS<sup>®</sup> APDL.

As mentioned earlier, the phonon peak influences the thermal conductivity calculation more prominently near  $T \sim 2$  K. In the first stage of this analysis, calculations were performed for the two models, considering  $T_B = 4.2$  K, where the phonon peak does not play a prominent role. Figure 7 shows variation of  $Q_0$  as a function of the applied magnetic field  $B_a$  for both MODEL-I and MODEL-II for a fixed value of  $\sigma_{no} \sim 6.897 \times 10^8 \Omega m^{-1}$ . Using the expression for  $RRR$  given in Refs.[1,5], this corresponds to  $RRR \sim 100$ . As seen in Fig. 7, the values of threshold magnetic field obtained for MODEL-I and MODEL-II are  $\sim 117$  mT and  $123$  mT respectively. At the threshold, the estimated temperature of the cavity inner surface is  $\sim 6.2$  K for MODEL-I. The highest value of the temperature estimated from the analysis on MODEL-II is  $\sim 6.24$  K. Unlike MODEL-I, the surface temperature is not constant throughout the surface of MODEL-II, instead there is a temperature profile, which is shown in Fig. 8.

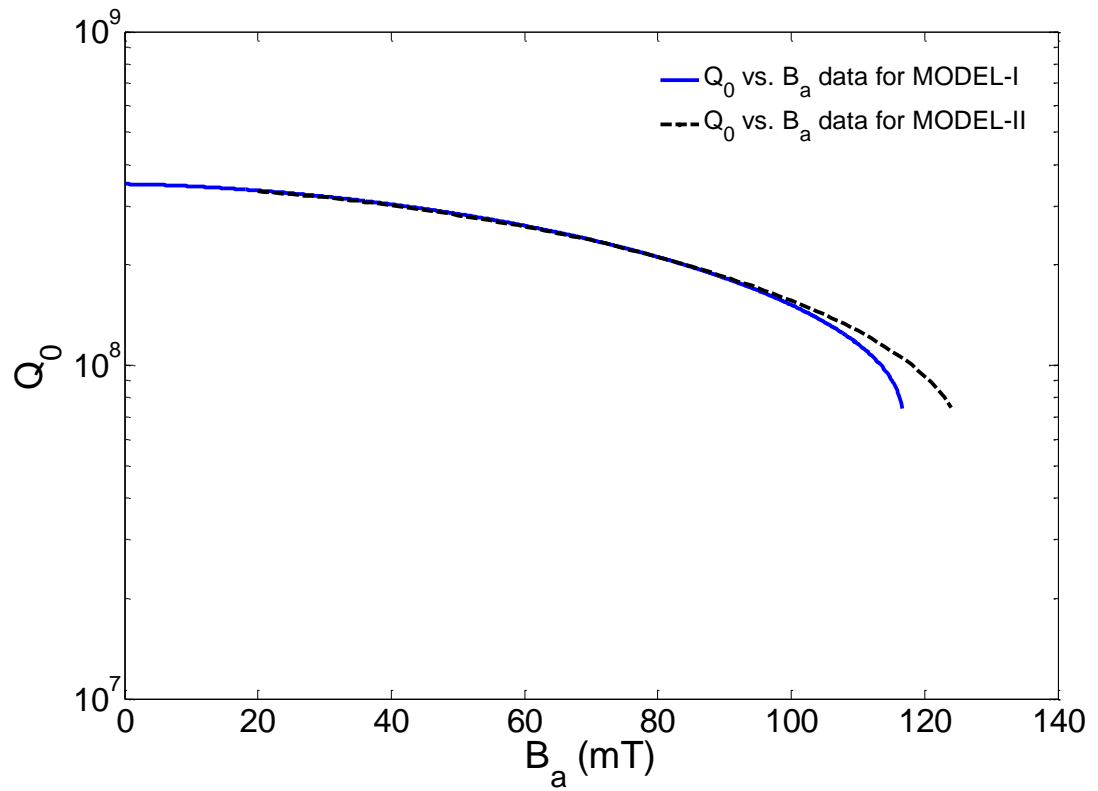


Fig. 7: Plot of  $Q_0$  as a function of  $B_a$ , as obtained from the analysis performed on MODEL-I (in blue) and MODEL-II (in black).  $Q_0$ -slope and  $Q_0$ -drop are clearly seen here.

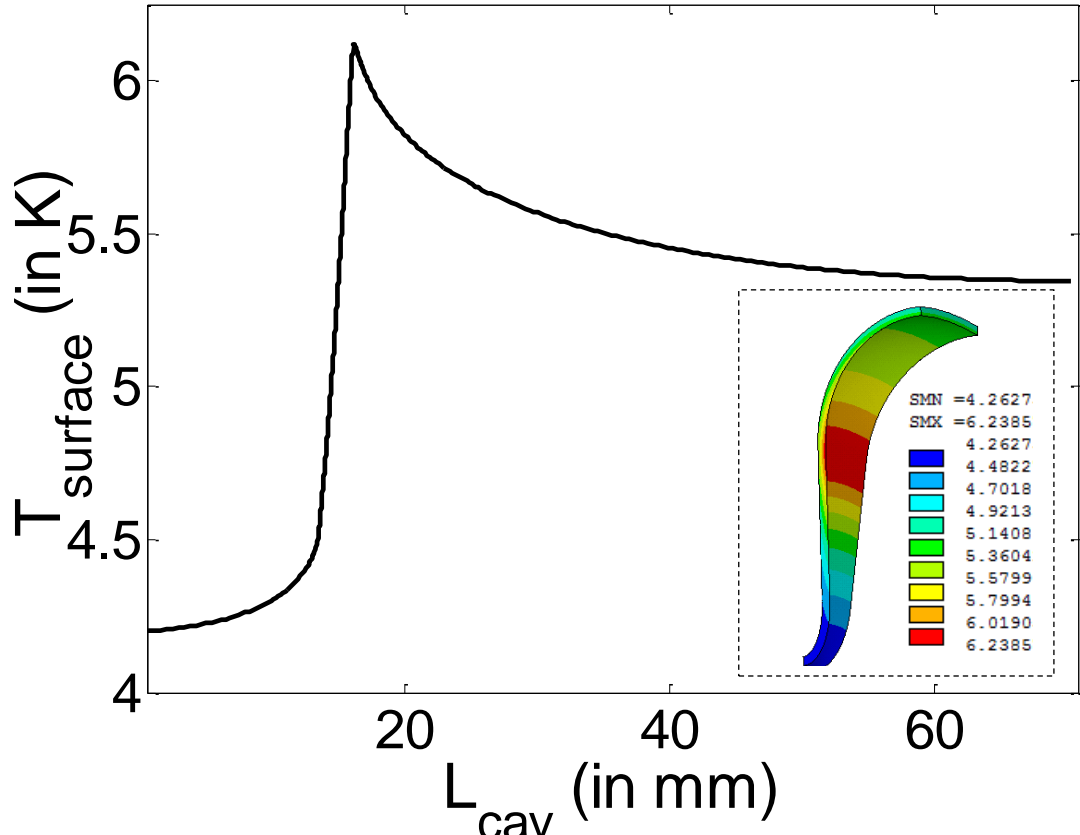


Fig. 8: Surface temperature variation along the length of the cavity, obtained for MODEL-II. Picture shown in the inset is the ANSYS generated surface profile of the temperature.

As we can see in Fig. 7, results obtained using these two models are quite close. This is expected because the heat flow is approximately one dimensional since the thickness of the cavity wall is much less compared to its lateral dimension. Hence, in the remaining of the paper, we perform the analysis for the simple plate geometry as described by MODEL-I.

The main objective of our analysis is to study the effect of the purity level of niobium on the threshold value  $B_{th}$  of the RF magnetic field at the SRF cavity surface. We have described in previous sections that the mean free path  $l_e$  of the normal electrons gives an estimation of the purity level of the material. However,  $l_e$  is not a directly measurable parameter. Hence, we can quantify the purity of the material in terms of  $\sigma_{no}$ , which is directly measurable. As we already described,  $l_e$  is proportional to  $\sigma_{no}$ . Therefore, in our analysis we have considered the parameter  $\sigma_{no}$  as an indicator for the purity level of the material and have calculated  $l_e$  from  $\sigma_{no}$  [20].

We present the calculations for  $T_B = 4.2 K as well as 2 K. We have considered the improved thermal conductivity  $\kappa$  due to the presence of phonon peak for 2 K. Figure 9 shows the variation of the  $Q_0$  as a function of  $B_a$  for MODEL-I, for a fixed value of  $\sigma_{no} \sim 6.897 \times 10^8 \Omega \text{ m}^{-1}$ . Here, the group of three closely spaced curves corresponds to the three different cases of phonon peak as described in Fig. 4 of the previous section, corresponding to 2 K case. As expected, the breakdown strength increases with the improvement in  $\kappa$ . For comparison, Fig. 9 also shows the case where phonon peak is ignored.$

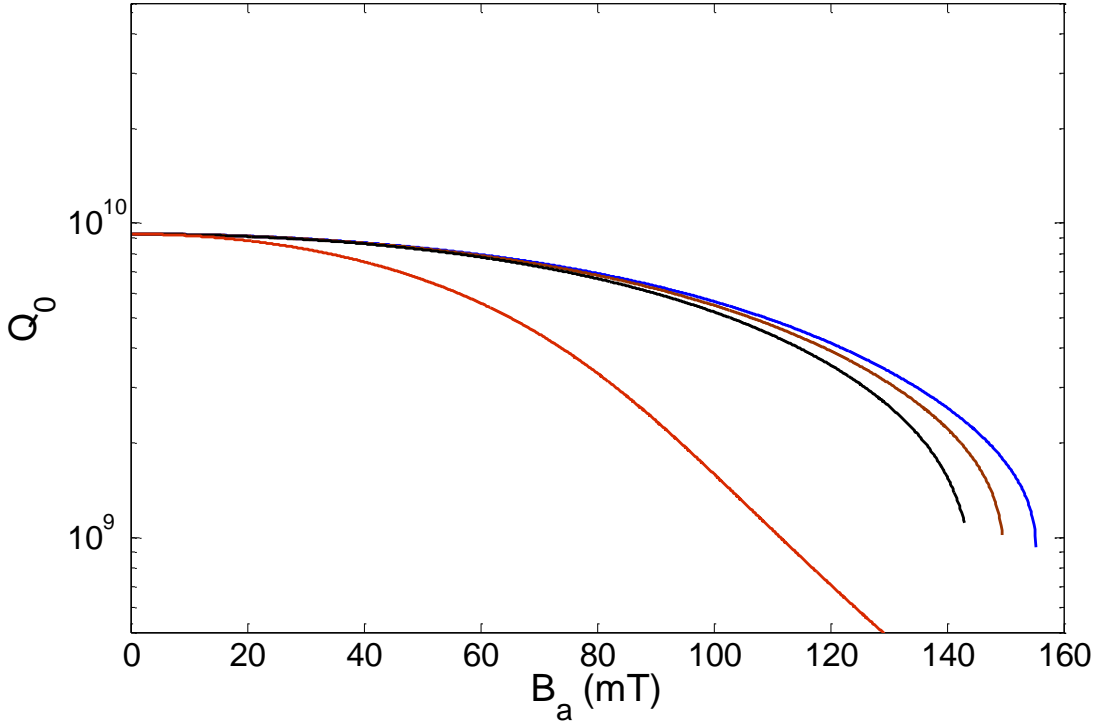


Fig. 9:  $Q_0$  is plotted as a function of the applied magnetic field  $B_a$ . The black, brown and blue curves correspond to the three cases of cavity processing corresponding to 2K as described in the text, where the estimated values of  $B_{th}$  are approximately 143 mT, 149 mT and 155 mT. The red curve corresponds to the case without phonon peak

Threshold values of the RF magnetic field  $B_{th}$  for different purity levels of the material were calculated, and the results are plotted in Fig. 10. In this analysis, we have used  $\sigma_{no}$  as an estimation of the purity level of the material. As we have already mentioned, the results corresponding to the bath

temperature  $T_B = 4.2$  K will have negligible effect of phonon peak. Hence, for all three samples, the results will be the same here. Plot of  $B_{th}$  as a function of  $\sigma_{no}$  is shown in Fig. 10 for the 4.2 K case. This plot shows a maximum of  $\sim 123$  mT at  $\sigma_{no} \sim 3.1 \times 10^8 \Omega m^{-1}$ , which corresponds to  $RRR \sim 45$ . Another three curves shown in Fig. 10, which are grouped together, give us the threshold magnetic field values as a function of  $\sigma_{no}$  for the 2 K case. As discussed earlier, the three curves represent the results corresponding to three different contributions of the phonon peaks, arising due to different processing levels of the material. As shown in the figure, the material that has undergone a heat treatment at  $1100^0$  C for 4 hrs, corresponds to a maximum of  $\sim 193$  mT, whereas for the two other cases, this value reduced to  $\sim 185$  mT and  $\sim 176$  mT respectively. Interestingly, all three maximum values correspond to a value of  $\sigma_n \sim 6.9 \times 10^7 (\Omega \cdot m)^{-1}$ , which corresponds to an  $RRR \sim 10$ .

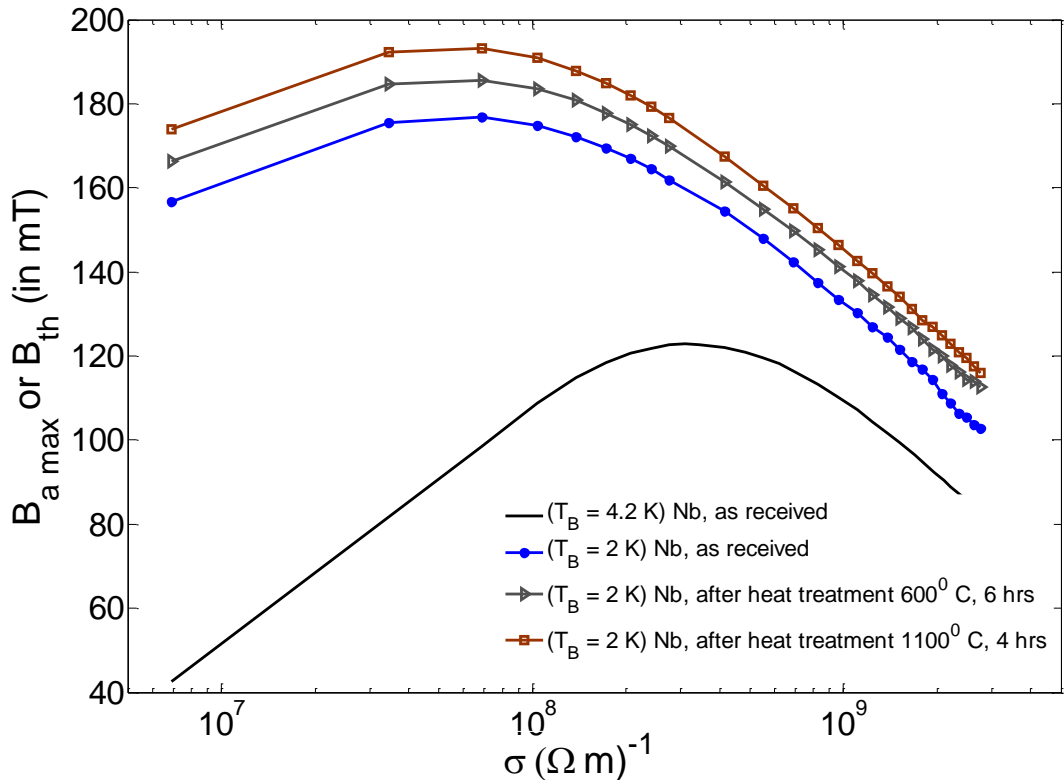


Fig. 10: Maximum attainable  $B_{th}$  as a function of  $\sigma_{no}$ . Here, the bulleted lines (CASE-I) corresponds to  $T_B \sim 2$  K results, and the smooth lines represents the situations when  $T_B \sim 4.2$  K.

#### IV. DISCUSSIONS AND CONCLUSIONS

In this paper, we have revisited the correlation between the purity level of the niobium SRF material, and the threshold magnetic field value  $B_{th}$  for breakdown of a SRF cavity. An increase in the purity level of the Nb material helps in achieving a higher thermal conductivity in its normal state. However, in the superconducting state and in the clean limit of superconductivity (as in the case of high  $RRR$  Nb materials), it is also associated with a simultaneous increase in the value of the superconducting surface resistance. Thus, this results in an ease in heat transfer, but with an added heat load. Therefore, to study the effect of purity on the Nb-SRF cavity performance, a rigorous thermal analysis was performed for a niobium cavity resonating at 650 MHz, considering the breakdown of the superconducting property of the material as a magneto-thermal phenomenon. In our analysis:

- (1)  $\sigma_{no}$  was used as a measure of the purity level of the Nb material.
- (2)  $R_s$  and  $\kappa$  were calculated as a function of  $T$ ,  $B_a$ , and the purity level of the material.
- (3) Kapitza resistance was estimated as a function of  $T$  and  $T_s$ .

In the first step of our analysis, we established that due to the small thickness of the cavity wall, the heat flows effectively in one direction, and hence we performed rest of the analysis on a simplified infinite plate geometric model of 4 mm thickness. From this analysis, considering  $T_B = 4.2$  K, we obtained a maximum of value of the threshold field  $B_{Th} \sim 123$  mT at  $\sigma_{no} \sim 3.1 \times 10^8 \Omega^{-1} m$ . Considering the bath temperature  $T_B = 2$  K, we analyzed three separate cases which correspond to three different stages of the SRF cavity post-processing, in order to realize the consequences of the modified  $\kappa$  in presence of the corresponding phonon peak. We found the maximum value of  $B_{Th} \sim 176$  mT, 185 mT and 193 mT respectively at a corresponding  $\sigma_{no} \sim 6.9 \times 10^7 \Omega^{-1} m$ . Interestingly, the corresponding values of  $RRR$  equivalent to these two  $\sigma_{no}$  values are  $\sim 45$  and  $10$  respectively. These values of  $RRR$  are much less compared to the  $RRR \sim 300$ , which is the specification for purity of niobium followed by the SRF community worldwide. From our literature study, we could not find a definite scientific basis behind the choice of  $RRR \sim 300$ . As mentioned in Ref. [30], the choice was based on the availability of pure Nb materials with a gross assumption of superior superconducting properties in such high purity materials. We thus believe that the choice of  $RRR \sim 300$  is somewhat empirical, which might have been chosen under certain conditions, and then the trend was continued. Based on our analysis, where we incorporated the purity of the Nb material as a variable parameter, we can argue that  $RRR \sim 300$  is indeed an over specification, and may be relaxed. There are some experimental results on SRF cavities that are made of niobium having  $RRR < 300$  [31], which convey a similar point. We believe that the reduction in the requirement of the purity level of niobium for SRF cavities can reduce the cost of the starting Nb material significantly.

Considering from the point of view of ease of availability,  $RRR \sim 100$ , *i.e.*, the reactor grade niobium can possibly be tested for the fabrication of SRF cavities. According to our analysis, this might help more to push the limit of the threshold magnetic field, as well as accelerating gradient further in the higher direction, compared to the conventional  $RRR \sim 300$  SRF cavities. Table-4 of ASTM B393 shows that the strength of the reactor grade niobium is 30% higher than that of RRR300 grade niobium. This gives further possibility of reducing the cavity thickness which benefits in two ways – (i) reducing peak temperature at cavity surface thereby increasing the threshold field and (ii) bringing down the material weight for each cavity.

At the low temperature regime, restoration of the phonon peak improves thermal conductivity  $\kappa$ . As observed experimentally, post-processing profoundly influences the lattice or the phonon contribution in  $\kappa$ . On the other hand, in the low temperature, even if the material is normal, the Wiedemann-Franz formula alone cannot predict the total electronic thermal conductivity  $\kappa_{en}(T)$ . An added contribution comes in the form of  $aT^2$ , as described by Eq. (7), which is significant at the low temperature. Although  $a$  can be estimated theoretically [22], it is not in good agreement with the experimental measured value. We have used the experimentally measured value of  $a$  in our analysis. As it is described in Section II, scale factor  $R(y)$  scales down  $\kappa_{en}(T)$  to  $\kappa_{es}(T)$ , when the material becomes superconductor. Therefore, instead of specifying only  $RRR$  for the starting Nb material, we suggest that  $\kappa(T)$  could also be an important parameter for Nb materials specification. Note that the  $\kappa(T)$  plays an important role in determining the diffusivity  $\alpha$  of the material. Here,  $\alpha = \kappa_{es}/\rho \times C_p(T)$ , where,  $\rho$  and  $C_p$  [32] are the density and specific heat of the material. We thus believe that instead of specifying the  $RRR$ , we should specify  $\sigma_{no}$ ,  $\kappa$  and  $\alpha$  of niobium to get full details of the material properties that determine the SRF cavity performance. Taking the reactor grade niobium as a material for cavity fabrication, we can specify these material parameters at 9.3 K as  $\sigma_{no} \sim 6.89 \times 10^8 \Omega^{-1} m$ , and  $\kappa \sim 138.68 \text{ W m}^{-1} \text{ K}^{-1}$  and  $\alpha \sim 0.005 \text{ m}^2 \text{ s}^{-1}$ . Here,  $C_p(T \sim 9.3 \text{ K}) = 3.36 \text{ J Kg}^{-1} \text{ K}^{-1}$ .

In our analysis, we have considered the global breakdown phenomenon of the superconducting property of the Nb material in the context of an SRF cavity. In some cases, the local effect like crack or micro-crack on the surface, inclusion of a large bead of normal or magnetic material and/or rough welding pits/bumps may also cause hot spots, which in turn can trigger the breakdown of

superconductivity of the material. Such extraneous effects can, however, be avoided by proper inspection and screening of starting Nb materials, and implementing careful SRF cavity fabrication and post processing techniques.

To conclude, we have analyzed the effect of material purity on the threshold RF magnetic field value  $B_{th}$  on the cavity surface that determines the maximum possible acceleration gradient in a Nb-based SRF cavity. Based on our analysis, we argue that  $RRR \sim 300$  grade niobium seems to be an over specification. This specification of Nb materials can be relaxed, which will have important implication in terms of a significant reduction in the cost of a Nb SRF cavity.

#### ACKNOWLEDGEMENTS

One of us (ARJ) would like to thank Amit Kumar Das for fruitful discussions.

#### References

- [1] Aune B., Bandelmann R., Bloess D. and Bonin B. *et. al.*, “*Superconducting TESLA cavities*”, Phys. Rev. ST Accel. Beams, vol. 3, 092001, Sep. 2000. DOI: <https://doi.org/10.1103/PhysRevSTAB.3.092001>
- [2] Kustom R. L., “*An overview of the Spallation Neutron Source project*”, Proc. 20th Int. Linear Accel. Conf., pp. 321-325, 2000. DOI: <http://arxiv.org/abs/physics/0008212>.
- [3] Henderson S., Abraham W., Aleksandrov A., and Allen C. *et. al.*, “*The Spallation Neutron Source accelerator system design*”, Nuclear Instruments and Methods in Physics Research A, Vol. 763, 1 Nov. 2014, pp 610–673. DOI: <http://dx.doi.org/10.1016/j.nima.2014.03.067>
- [4] Boussard D., and Linnecar T., “*The LHC superconducting RF system*”, LHC Project Report 316, Presented at CEC-ICMC'99, 12-16 July 1999, Montreal, Canada.
- [5] H. Padamsee, J. Knobloch, and T. Hays, “*RF Superconductivity for Accelerators*”. New York, NY, USA: Wiley, 1998.
- [6] Roy S. B., and Myneni G. R., “*Qualification of niobium materials for superconducting radio frequency cavity applications: View of a condensed matter physicist*”, AIP Conf. Proc., Vol 1687, Issue 1, DOI: <http://dx.doi.org/10.1063/1.4935320>
- [7] T. P. Wangler, *Principles of RF Linear Accelerators*. New York, NY, USA: Wiley, 1998, Wiley Series in Beam Physics and Accelerator Technology ISBN 0-471-16814-9.
- [8] Ciovati G., Myneni G., Stevie F., and Maheshwari P. *et. al.*, “*High field Q slope and the baking effect: Review of recent experimental results and new data on Nb heat treatments*”, Phys. Rev. ST Accel. Beams, vol. 13, 022002, 2010, DOI: [10.1103/PhysRevSTAB.13.022002](https://doi.org/10.1103/PhysRevSTAB.13.022002)
- [9] Ciovati G., “*Review of the frontier workshop and Q-slope results*”, Physica C 441 (2006) 44–50, DOI: [10.1016/j.physc.2006.03.126](https://doi.org/10.1016/j.physc.2006.03.126)
- [10] M. Tinkham, “*Introduction to Superconductivity*”, 2<sup>nd</sup> Edition, New York, NY, USA: Dover Pub. 2004.
- [11] Ciovati G., “*AC/RF superconductivity*”, CERN Yellow Report CERN-2014-005, (2015), pp.57-75 DOI: [10.5170/CERN-2014-005.57](https://cds.cern.ch/record/1120310/files/p219.pdf)
- [12] W. Weingarten. “*Handbook of Applied Superconductivity*”1998, Volume.2 Ed. B. Seeber (IOP Publishing Ltd.), p1381.]
- [13] T. L. Francavilla, R.A. Hein, and D. H. Liebenberg, (Eds.), “*Magnetic Susceptibility of Superconductors and Other Spin Systems*”, 1<sup>st</sup> Edition, USA: Springer. 1991, DOI: [10.1007/978-1-4899-2379-0](https://doi.org/10.1007/978-1-4899-2379-0)
- [14] Safa H., “*High gradient in SCRF cavities*”, Particle Accelerators, Vol. 60, (1998), pp. 219-230, DOI: <https://cds.cern.ch/record/1120310/files/p219.pdf>
- [15] Kim S. H. and Campisi E. I., “*Thermal stabilities and optimal operating parameters for the Oak Ridge Spallation Neutron Source superconducting linear accelerator*”, Phys. Rev. ST Accel. Beams, vol. 10, 032001 (2007). DOI: [10.1103/PhysRevSTAB.10.032001](https://doi.org/10.1103/PhysRevSTAB.10.032001)
- [16] Weingarten W., “*Field-dependent surface resistance for superconducting niobium accelerating cavities*”, Phys. Rev., Vol. 14, 101002 (2011).
- [17] Gurevich A., “*Multiscale mechanisms of SRF breakdown*”, Physica C 441 (2006) 38–43, DOI: [http://dx.doi.org/10.1016/j.physc.2006.03.024](https://doi.org/10.1016/j.physc.2006.03.024)
- [18] Jana A. R., Kumar V, Kumar A., and Gaur R., “*Electromagnetic Design of a  $\beta_g = 0.9$  650-MHz Superconducting-Radio-Frequency Cavity*”, IEEE Trans. Applied Superconductivity, Vol. 23, Issue. 4, May-2013, pp. 3500816 -3500816, (2013). DOI: [10.1109/TASC.2013.2256356](https://doi.org/10.1109/TASC.2013.2256356)
- [19] Jana A. R. and Kumar V, “*On the Electromagnetic Design of a  $\beta_g = 0.61$ , 650 MHz Superconducting Radiofrequency Cavity*”, IEEE Trans. Applied Superconductivity, Vol. 24, Issue. 6, Dec. 2014, pp. 1-16, Dec. 2014. DOI: [10.1109/TASC.2014.2332435](https://doi.org/10.1109/TASC.2014.2332435)

[20] Goodman B. B., and Kuhn G., “*Influence of Extended Defects on the Superconductive Properties of Niobium*” J. Phys. Paris, 29(240), 1968.

[21] N. W. Ashcroft and N. D. Mermin, “Solid State Physics”, 9<sup>th</sup> Indian Reprint, New Delhi, India, Cengage Learning, 2010.

[22] F Koechlin and B Bonin, “*Parametrization of the niobium thermal conductivity in the superconducting state*”, Supercond. Sci. Technol., Vol. 9, Number 6, (1996), pp-453-460

[23] Sharath Chandra L. S., Chattopadhyay M. K., Roy S. B., and Sahni V. C. *et. al.*, “*Magneto thermal conductivity of superconducting Nb with intermediate level of impurity*”, Supercond. Sci. and Tech., Vol 25, Issue 3, 035010, 12 pp. (2012); DOI: [10.1088/0953-2048/25/3/035010](https://doi.org/10.1088/0953-2048/25/3/035010)

[24] Bardeen J., Rickayzen G., and Tewordt L., “*Theory of the Thermal Conductivity of Superconductors*”, Phys. Rev. 113, 982 –15 February 1959; DOI: <https://doi.org/10.1103/PhysRev.113.982>

[25] Chandrasekaran S. K., Bieler T., Compton C., and Wrightnt N. T., “*Phonon scattering in the thermal conductivity of large-grain superconducting niobium as a function of heat treatment temperature*”, AIP, 1434, 976 (2012); DOI: [10.1063/1.4707015](https://doi.org/10.1063/1.4707015)

[26] Mittag H., “*Kapitza conductance and thermal conductivity of copper niobium and aluminum in the range from 1.3 to 2.1 K*”, Cryogenics 13 (1973) 94.

[27] Ballantini R., Chincarini A., Gemme G., and Parodi R., “*Pipe cooling perspectives for superconducting accelerating cavities*”, Phys. Rev. STAB, 6, 083201 –29 August 2003; DOI: [10.1103/PhysRevSTAB.6.083201](https://doi.org/10.1103/PhysRevSTAB.6.083201)

[29] Belomestnykh S., Shemelin V., “*High- b cavity design—A tutorial*”, Proc. 12<sup>th</sup> Int. Workshop RF Supercond., pp. 2-19, 2005, DOI: <http://www.lepp.cornell.edu/public/SRF/2006/SRF060424-03/SRF060424-03.pdf>

[30] Singer W., Singer X., Brinkmann A., and Iversen J. *et. al.* “*Superconducting cavity material for the European XFEL*”, Supercond. Sci. Technol. 28-085014 (2015).

[31] Dhakal P., Ciovati G., Kneisel P., and Myneni G. R., “*Enhancement in Quality Factor of SRF Niobium Cavities by Material Diffusion*”, IEEE Trans. Applied Superconductivity, Vol. 25, Issue. 3, June 2015, 3500104, (2015). DOI: [10.1109/TASC.2014.2359640](https://doi.org/10.1109/TASC.2014.2359640)

[32] Leupold H. A., and Boorset H. A., “*Superconducting and normal specific heats of a single crystal of niobium*”, Phys. Rev., Vol. 134, Num.-5A, 1 June, 1964